A General Approach to Programmable and Reconfigurable Emulation of Power Impedances

Sinan Li, *Member, IEEE*, Wenlong Qi, *Student Member, IEEE*, Siew-Chong Tan, *Senior Member, IEEE*, S. Y. Hui, *Fellow, IEEE*, and Chi K. Tse, *Fellow, IEEE*

***Abstract*—Starting with a brief review on the existing methods of impedance emulation, this paper addresses a general and systematic approach to programmable and reconfigurable emulation of power impedances. The proposed approach not only enables the impedance value to be programed, but also allows the characteristics (i.e., type) of the impedance to be reconfigured instantly during the operation. Based on the proposed control method, emulation of at least six types of emulated power impedances (EPI) can be easily attained. In particular, it is theoretically and practically demonstrated that the impedance characteristic can be emulated through a combination of different functions. The systematic derivation of these functions is explained. New techniques that compensate the circuit power losses are introduced. This general approach has been practically verified in several EPI. Both steady-state and dynamic performance of these EPI confirm the programmability and reconfigurability. It is envisaged that the proposed method can be applied to a range of functions, such as power filtering, energy storage, and even power conversion based on direct impedance control.**

***Index Terms*—Hardware-in-the-loop, impedance emulation, programmable impedance, static var compensator.**

I. Introduction

An EMULATED power impedance (EPI) is a two-terminal power-electronic device that can actively mimic the exact voltage–current characteristic of a physical passive component (see Fig. 1). The basic principle of an EPI is to control the power electronics such that its terminal current i_f and terminal voltage v_f satisfy

$$i_f(s) = \frac{v_f(s)}{Z_e(s)} \tag{1}$$

where $Z_e(s)$ is the transfer function that defines the characteristic impedance in the s domain.

Manuscript received September 23, 2016; revised December 16, 2016; accepted January 24, 2017. Date of publication February 2, 2017; date of current version October 6, 2017. This work was supported by the Hong Kong Research Grant Council under the theme-based Research Project T23-701/14-R/N. Recommended for publication by Associate Editor Dr. Giovanna Oriti.

S. Li, W. Qi, S.-C. Tan, and S. Y. R. Hui are with the Department of Electrical and Electronic Engineering, The University of Hong Kong, Pokfulam, Hong Kong (e-mail: snli@eee.hku.hk; wlqi@eee.hku.hk; sctan@eee.hku.hk; ronhui@eee.hku.hk).

C. K. Tse is with the Department of Electronic and Information Engineering, Hong Kong Polytechnic University, Pokfulam, Hong Kong (e-mail: michael.tse@polyu.edu.hk).

Color versions of one or more of the figures in this paper are available online at http://ieeexplore.ieee.org.

Digital Object Identifier 10.1109/TPEL.2017.2663424

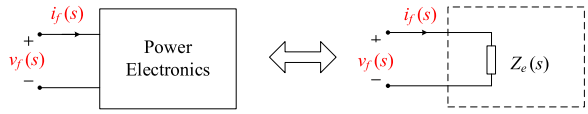

Fig. 1. EPI $Z_e(s)$ based on power electronics.

The concept of EPI is not new. The earliest attempt to use an EPI can be traced back to the input current shaper for active power factor correction applications in the early 1900's, where the power converter turns its associated load into an emulated resistor [1]. Over the past years, the concept of EPI is quickly evolving and has been widely employed for many power electronics and power system applications. One immediate application is to directly replace physical power impedances, because an EPI built from advanced semiconductors and control techniques can be made more compact, lightweight [2]–[4], (possibly) more reliable [5], [6], and being capable of varying its impedance value [4], [7]–[9]. For instance, an emulated inductor has been reported as a direct replacement of the heavy dc-link inductor for adjustable speed drive applications [4] and a variable line impedance emulator for hardware-in-the-loop applications [7]. An emulated capacitor has been used to replace the unreliable dc-link capacitors [2] and to stabilize the distributed dc power supply system [8]. Another major application of EPI is to provide power flow control and ancillary services, such as active power filtering and var compensation for power system applications [9]–[11]. It has been demonstrated that the control structure of an EPI can be simpler than that of the existing control methods. Presently, an EPI can only be designed to perform a single task because it can only emulate a fixed type of impedance at a time. As a result, the potential of EPI is somehow constrained. One example is the use of EPI as a static var compensator (SVC). Reported EPI can only generate capacitive or inductive reactive power, because of its inability to interchange between a capacitive and an inductive mode of operation. In this case, a programmable EPI (of which not only the value of its impedance, but also its type can be easily reconfigured) will be highly desirable for achieving a true SVC, through which both types of reactive power can be generated. A programmable EPI may also be useful as a multifunctional equipment, of which the functions can be conveniently defined by users according to the required tasks. Although it has been predicted in theory that any EPI can be synthesized based on (1) [12], the issues and solutions toward achieving a practical programmable EPI have not been reported in the prior works.

In this paper, the programmable and reconfigurable aspects of a general EPI are systematically examined and explored. The objective is to identify and resolve the technical issues toward a general and reconfigurable impedance emulation method. According to [12], the emulation of general impedance requires a minimum of two power converters (one for programming the input voltage and current relationship, and the other for balancing the active and reactive power). For illustration purposes, only a programmable and reconfigurable power reactance is constructed to prove the concept. Since no real power generation is needed (theoretically), only one power converter can be employed if the output termination is chosen appropriately to facilitate the power balance. This makes the characterization (e.g., the control method, the bandwidth) of an EPI easier. In Section II, the existing EPI technologies for emulating various power reactances are briefly reviewed and the issues toward achieving a programmable EPI are described. In Section III, a direct reference generation method that is critical in accomplishing the goal of a programmable EPI is presented. In Section IV, several critical design considerations regarding the hardware design, the control, and their effects on the actual EPI performance are explained. Finally, a dynamically programmable and reconfigurable (multifunctional) EPI is used to demonstrate the general principle of this systematic approach in Section V.

II. Review of Emulated Power Reactances

A. Types of Emulated Power Reactances

If emulated resistance is not considered, a programmable reactance can be classified into three categories:

1) *Linear inductor/capacitor:* A linear inductor/capacitor has a positive and frequency-independent inductance/capacitance value (represented as curve ① in Fig. 2). Physical inductors/capacitors belong to this category. An emulated linear inductor/capacitor is useful for replacing its physical counterparts in applications, where size, weight, and sometimes reliability are of major concern. Both dc and ac versions of emulated linear inductor/capacitor have been reported [4], [7], [8], [12], [13].
2) *Negative inductor/capacitor:* Like a linear inductor/ capacitor, a negative inductor/capacitor also has a frequency independent inductance/capacitance profile except that its value is negative (represented as curve ②in Fig. 2). These types of impedance do not exist physically. Previously, a negative inductor has been emulated [14], but no similar work has been reported for the negative capacitor. Applications of a negative inductor include the cancellation of the voltage drop attributed to line inductance along the transmission line.
3) *Frequency-dependent inductor/capacitor:* As illustrated in curve ③in Fig. 2, typical frequency-dependent inductor/capacitor usually has inductance/capacitance values around some selective bandpass frequencies (such as ω_{r1}, ω_{r2}). This type of EPI can be used in the forms of an SVC, an active filter, and many other types of FACTS devices through which compensating power at selective frequencies (e.g., the fundamental and/or its higher harmonic frequencies) are generated [9]–[11].

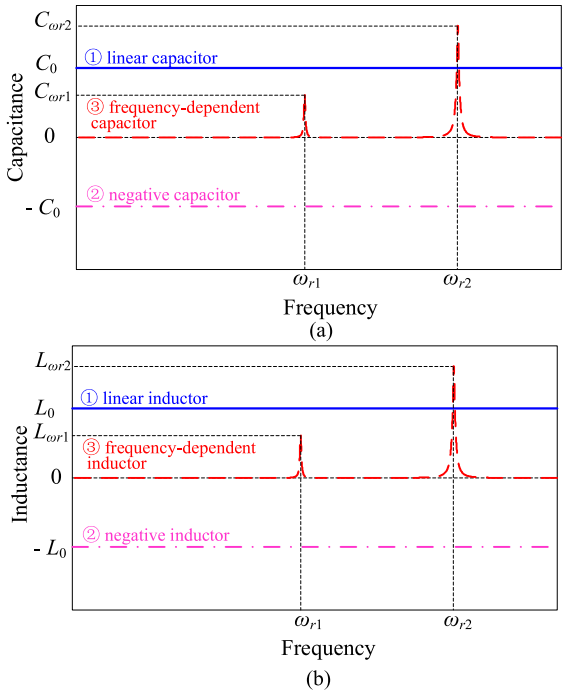

Fig. 2. Illustration of (a) a linear capacitor, a negative capacitor, a frequency-dependent capacitor, and (b) a linear inductor, a negative inductor, a frequency-dependent inductor in the frequency domain.

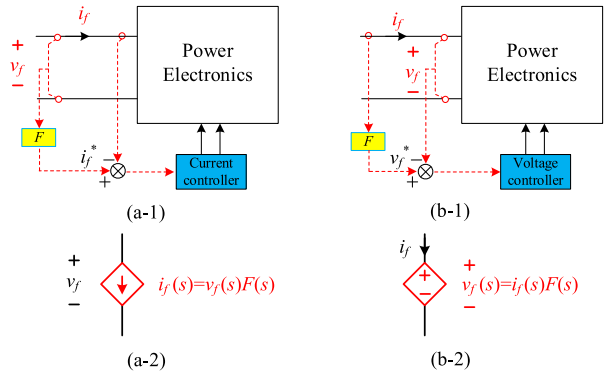

Fig. 3. Control diagram of an EPI based on (a-1) voltage-controlled current source method and (b-1) current-controlled voltage source method, together with their equivalent electrical models (a-2) and (b-2), respectively.

B. Issues of the Existing Control Methods for Achieving Programmable EPIs

Fig. 3(a) and (b) shows the control block diagrams of the existing EPIs under current-control and voltage-control schemes, respectively. Current control involves the control of the terminal current i_f based on the measured terminal voltage v_f [see Fig. 3(a)] to follow a reference signal i_f^*. Voltage control requires a voltage reference of v_f^* and the regulation of the terminal voltage v_f based on the measured i_f [see Fig. 3(b)]. Essentially, an EPI based on these methods becomes a (terminal) current-controlled voltage source (CCVS) [see Fig. 3(a-2)]

TABLE I
IMPEDANCE CONTROL FUNCTION *F* FOR EMULATING VARIOUS POWER REACTANCES

EPI Type \ Control method	Impedance Control Function *F*: Voltage controlled current source	Impedance Control Function *F*: Current controlled voltage source
Linear capacitor (C_e)	$sC_e(s)$	$1/[sC_e(s)]$
Linear inductor (L_e)	$1/[sL_e(s)]$	$sL_e(s)$
Negative capacitor (-C_e)	$-sC_e(s)$	$-1/[sC_e(s)]$
Negative inductor (-L_e)	$-1/[sL_e(s)]$	$-sL_e(s)$
Frequency-dependent capacitor	Achieved in *dq* rotating frame	
Frequency-dependent inductor		

or a (terminal) voltage-controlled current source (VCCS) [see Fig. 3(b-2)]. In both methods, the reference signals are generated through an impedance control function *F*. If the desired impedance to be emulated has an *s*-domain transfer function of $Z_e(s)$, then *F* should satisfy

$$F(s) = 1/Z_e(s) \tag{2}$$

for VCCS method, and

$$F(s) = Z_e(s) \tag{3}$$

for CCVS method, where *F*(*s*) is the *s*-domain expression of *F*. The *F*(*s*) in (2) and (3) for four different types of impedances are summarized in Table I. For frequency-dependent inductor/capacitors, however, they cannot be expressed in terms of $Z_e(s)$ due to its frequency-dependent profile. Conventionally, *F* is realized by manipulating the phasor of i_f or v_f in a rotating *dq* frame [7], [9]–[11].

From Table I, the issues of the existing control methods toward achieving a programmable emulated power reactance can be identified as follows:

1) The impedance control function for many emulated power reactance contains a differentiator or an integrator. The use of a differentiator could lead to noise issues in the control circuit [6], [8], while the use of an integrator could introduce undesirable dc-offset into the reference signal which must be properly compensated [4], [7], [13], [14]. The presence of differentiator or integrator makes the practical EPI implementation cumbersome and the resulting dynamic performance poor. This explains why most existing EPI are designed with a fixed impedance value and are applied under a single operating condition.
2) Each type of EPI requires a distinctive impedance control function for reference generation. It is therefore not straightforward to change the impedance type of an EPI. At present, no EPI that can emulate several types of impedances has been reported.

The abovementioned analysis indicate that, in order to achieve true programmability, a simple EPI control method which (i) does not involve differentiators or integrators, and (ii) can be easily configured to emulate different types of EPI will be required.

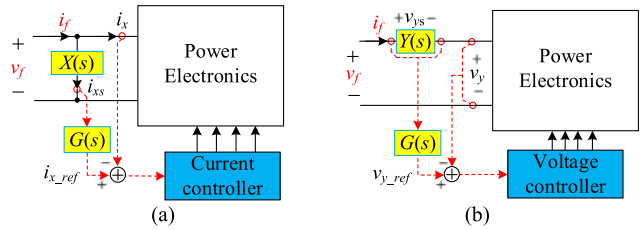

Fig. 4. Direct reference generation technique for emulating power impedance based on (a) current-control current source method, and (b) voltage-control voltage source method.

III. PROPOSED SOLUTION BASED ON DIRECT REFERENCE GENERATION

A. Basic Principles of Direct Reference Generation

A generalized approach to emulating power impedance is described in this section for the current- and voltage-control schemes. Fig. 4(a) shows one proposed approach to controlling the EPI by direct reference generation. Different from the methods described in Fig. 3(a), the method here does not require a differentiator or integrator. Instead, it involves only a voltage sensing network, i.e., the parallel impedance *X*(*s*) and a simple impedance control function *G*(*s*) to generate the current reference signal. In particular,

$$i_{x\_\mathrm{ref}}(s) = i_{xs}(s)\,G(s) \tag{4}$$

where $i_{xs}(s)$ is the current of the sensing impedance *X*(*s*) and $i_{x\_\mathrm{ref}}(s)$ is the reference of the input current of the power converter $i_x(s)$.

If a perfect current controller is assumed, i.e., $i_{x\_\mathrm{ref}}(s) = i_x(s)$, then

$$i_f(s) = i_{xs}(s) + i_x = [G(s)+1]\,i_{xs}(s). \tag{5}$$

As a result, the impedance $Z_e(s)$ which the system emulates (including the effect of *X*(*s*)) is

$$Z_e(s) = \frac{v_f(s)}{i_f(s)} = \frac{v_f(s)}{[G(s)+1]\,i_{xs}(s)} = \frac{X(s)}{G(s)+1}. \tag{6}$$

In its simplest form with $G(s) = K$ (*K* is a positive constant), (6) becomes

$$Z_e(s) = \frac{1}{(K+1)\frac{1}{X(s)}}. \tag{7}$$

According to (7), the reciprocal (or the admittance) of $Z_e(s)$ is an amplified version ($K+1$ times amplification) of the admittance of *X*(*s*). If a small capacitor C_o is used as the sensing impedance, i.e., $X(s) = 1/(sC_o)$, then the emulated impedance is simply

$$Z_e(s) = \frac{1}{(K+1)(sC_o)} = \frac{1}{s[(K+1)C_o]} = \frac{1}{sC_e} \tag{8}$$

in which the equivalent capacitor C_e has a capacitance value of $(K+1)C_o$. In this way, a linear capacitor can be emulated

without taking a differentiation or integration. By adjusting the parameter K, one is able to change the capacitance value conveniently.

Based on the duality principle, another form of the impedance emulation method can be derived as shown in Fig. 4(b), in which a series current sensing impedance $Y(s)$ is employed to generate the voltage reference $v_{y\_\mathrm{ref}}(s)$. Assuming perfect voltage control, i.e., $v_{y\_\mathrm{ref}}(s) = v_y(s)$, $Z_e(s)$ becomes

$$Z_e(s) = \frac{v_f(s)}{i_f(s)} = [G(s)+1]\frac{v_{ys}(s)}{i_f(s)} = [G(s)+1]Y(s). \tag{9}$$

If $G(s) = K$, then

$$Z_e(s) = (K+1)Y(s). \tag{10}$$

Equation (10) means that $Z_e(s)$ is a "$K+1$" amplified version of $Y(s)$. It implies that a small inductor L_o can be used as a sensing impedance to emulate a large linear inductor L_e with inductance value of $(K+1)L_o$. Again, no differentiation or integration is needed in this method.

Essentially, an EPI based on the abovementioned methods becomes a current-controlled current source (CCCS) in Fig. 4(a), or a voltage-controlled voltage source (VCVS) in Fig. 4(b). The proposed control strategy enables a direct generation of the reference signal without the need for phase conversion which is originally achieved through an integrator/differentiator. Thus, the delay in reference signal generation is minimal. This will significantly improve the dynamic accuracy of the impedance emulation [7].

B. Towards a Programmable EPI

A fully programmable and reconfigurable EPI should allow not only the value, but also the type of the EPI to be changed. According to (6) and (9), the type of EPI can be controlled by changing $G(s)$. For (6), if $X(s) = 1/(sC_o)$, and

1) $G(s) = k_p$, then $Z_e(s) = 1/[s(k_p+1)C_o]$;
2) $G(s) = -k_p$, then $Z_e(s) = 1/[s(1-k_p)C_o]$;
3) $G(s) = \frac{k_r\omega_c s}{s^2+\omega_c s+\omega_r^2}$, then $Z_e(s) = \frac{1}{sC_o\left[\frac{s^2+(k_r+1)\omega_c s+\omega_r^2}{s^2+\omega_c s+\omega_r^2}\right]}$;
4) $G(s) = \frac{-k_r\omega_c s}{s^2+\omega_c s+\omega_r^2}$, then $Z_e(s) = \frac{1}{sC_o\left[\frac{s^2+(1-k_r)\omega_c s+\omega_r^2}{s^2+\omega_c s+\omega_r^2}\right]}$.

In these four cases, $G(s)$ is a proportional (P) function, a negative proportional function ($-P$), a second-order resonant (R) function, and a negative second-order resonant ($-R$) function, respectively. It can be concluded that:

1) If G(s) is a P function, then $Z_e(s)$ is a *linear capacitor* with capacitance value of $(k_p+1)C_o$, as given previously in (8);
2) If G(s) is a $-P$ function, then $Z_e(s)$ is a *negative capacitor* with capacitance value of $(1-k_p)C_o$ (assume that $k_p \geq 1$). If $k_p \gg 1$, then the negative capacitor here possesses almost the same impedance magnitude as the linear capacitor in (i), except that the phase is shifted by 180°.
3) If G(s) is an R function, then $Z_e(s)$ is a *quasi-frequency-dependent capacitor,* because it has a capacitance of $(k_r+1)C_o$ at frequency ω_r, since

$$Z_e(s)|_{s=j\omega_r} = \frac{1}{j\omega_r C_o(k_r+1)} \tag{11}$$

and a capacitance of C_o at low frequencies (when $s \ll 1$) or at high frequencies ($s \to \infty$), $Z_e(s)$ since

$$Z_e(s)|_{s\ll 1} = Z_e(s)|_{s\to\infty} = \frac{1}{sC_o}. \tag{12}$$

If C_o is sufficiently small such that $Z_e(s)$ is almost like an open circuit at the low-frequency range and the passing band of the R function defined by ω_c is narrow, then the quasi-frequency-dependent capacitor can be used to approximate an ideal frequency-dependent capacitor.

1) If G(s) is an $-R$ function, then $Z_e(s)$ is a *quasi-frequency-dependent inductor* with an effective inductance of $1/(\omega_r^2 C_o(k_r-1))$ at frequency ω_r. At low frequencies (when $s \ll 1$) or at high frequencies ($s \to \infty$), $Z_e(s)$ is equivalent to a capacitor with a capacitance value of C_o. Analogous to (iii), a quasi-frequency-dependent inductor can be used to approximate an ideal frequency-dependent inductor, provided that C_o is sufficiently small and the passing band of the $-R$ function is narrow.

The frequency responses of Z_e (in the form of admittance) based on $C_o = 10\,\mu$F, $k_p = 100$, $k_r = 100$, $\omega_r = 628$ rad/sec, and $\omega_c = 0.628$ rad/sec, when $G(s)$ is configured as a P, $-P$, R and $-R$ function are calculated and shown in Fig. 5. With a P and $-P$ impedance control function, $Z_e(s)$ is emulating a linear capacitor of 1010 μF and a negative capacitor of $-990\,\mu$F, respectively. When $G(s)$ is an R function, $Z_e(s)$

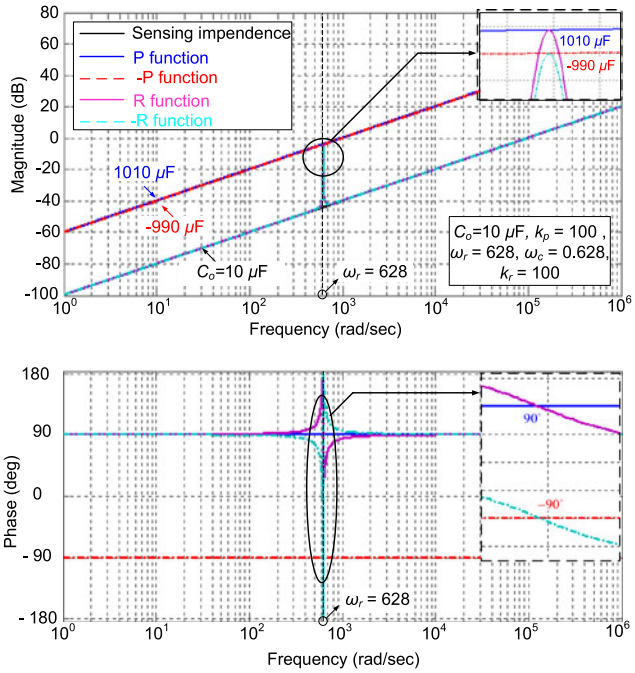

Fig. 5. Frequency responses of the EPI $Z_e(s)$ (in the form of admittance), given the impedance control function $G(s)$ configured as a P function, a $-P$ function, a second-order R function (with a pair of resonant poles at ω_r), and a second-order $-R$ function (with a pair of resonant poles at ω_r).

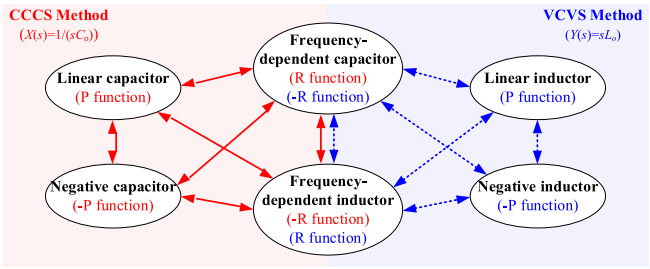

Fig. 6. Transitional diagram among various EPIs.

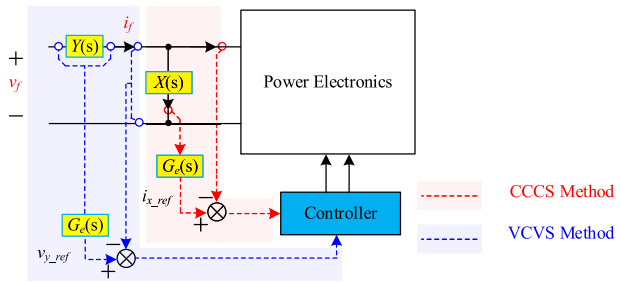

Fig. 7. Combined CCCS–VCVS method, which incorporates a parallel sensing and a series sensing impedance $X(s)$ and $Y(s)$.

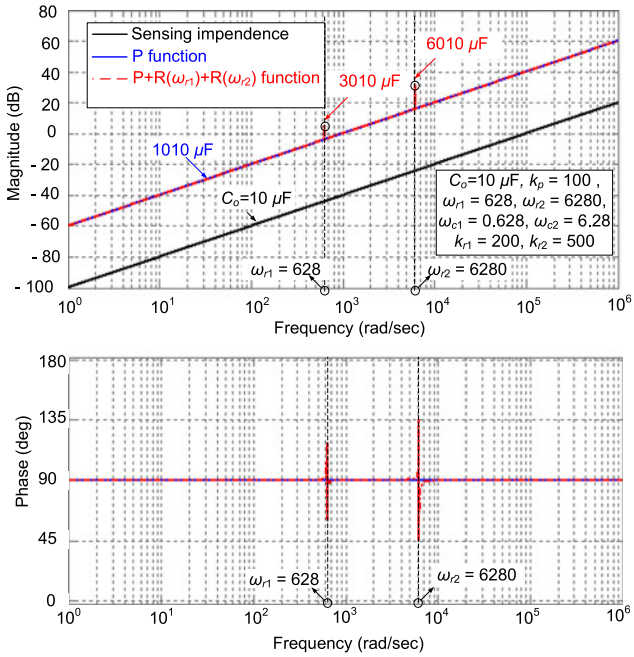

Fig. 8. Frequency responses of the EPI $Z_e(s)$ (in the form of admittance), when the impedance control function $G(s)$ contains one P term and two second-order R terms (with two pairs of resonant poles at $\omega_{r1} = 628$ and $\omega_{r2} = 6280$).

is a quasi-frequency-dependent capacitor, since the frequency responses of $Z_e(s)$ overlaps with the $C_o = 10\,\mu$F admittance line for all frequencies except at $\omega_r = 628$ rad/sec, when it intersects with the 1010-μF admittance line. Finally, when $G(s)$ is an $-R$ function, $Z_e(s)$ is a quasi-frequency-dependent inductor with an inductance of 2.56 mH at $\omega_r = 628$ rad/sec and a capacitance of $C_o = 10\,\mu$F at other frequencies. The frequency-dependent impedance profile together with its almost zero admittance of at the low-frequency ranges (and thus nearly null responses at these frequencies) offers the feasibility of using a quasi-frequency-dependent capacitor/inductor to approximate an ideal frequency-dependent capacitor/inductor.

By configuring $G(s)$ as a P, $-P$, R, or $-R$ function, the EPI can be flexibly changed between a *linear capacitor*, a *negative capacitor*, a *quasi-frequency-dependent capacitor,* or a *quasi-frequency-dependent inductor* based on CCCS method (see Fig. 6). Note that $G(s)$ can also be configured to emulate a linear inductor and a negative inductor. This will require $G(s)$ to incorporate two integrators which are undesirable. Alternatively, if the VCVS method shown in Fig. 4(b) is employed, then based on (9) and assuming $Y(s) = sL_o$, $Z_e(s)$ can be easily configured as a *linear inductor*, a *negative inductor*, a *quasi-frequency-dependent inductor,* or a *quasi-frequency-dependent capacitor* by configuring $G(s)$ as a P, $-P$, R, or $-R$ function, respectively (see Fig. 6).

It should be noted that each emulation method given in Fig. 4 can emulate four types of EPI. If all the six types of EPI are needed, a combined system augmented with both series and parallel sensing impedances can be employed (as shown in Fig. 7). A complete emulation of the six types of EPI can be achieved by switching between the CCCS and VCVS mode of operation.

C. Further Extensions of Programmability and Reconfigurability

$G(s)$ may be further configured as a combination of the four functions (P, $-P$, R, and $-R$), e.g., $P + R$, $P - R$, $-P + R$, $-P + R$, etc. For instance, if $G(s) = k_p + \frac{k_{r1}\omega_c s}{s^2+\omega_c s+\omega_{r1}^2} + \frac{k_{r2}\omega_c s}{s^2+\omega_c s+\omega_{r2}^2}$, which contains one P function and two R functions, then based on CCCS method and assuming $X(s) = 1/(sC_o)$, the frequency response of $Z_e(s)$ can be illustrated as shown in Fig. 8.

Due to the P term in $G(s)$, $Z_e(s)$ behaves like a linear capacitor with a capacitance value of $(k_p + 1)C_o$ (i.e., 1010 μF) for all frequencies. The two R terms, on the other hand, provide an additional capacitance gain at the frequencies of ω_{r1} and ω_{r2}. The equivalent capacitance is, therefore, increased to $(k_p + k_{r1} + 1)C_o$ (i.e., 3010 μF) at ω_{r1}, and $(k_p + k_{r2} + 1)C_o$ at ω_{r2} (i.e., 6010 μF). The inclusion of multiple R functions may be useful for filtering out high order harmonics in power system applications as an active filter.

IV. Design Considerations

A. Hardware Design Considerations

Fig. 9(a-1) and (b-1) illustrate how to use a full-bridge converter to setup an EPI based on the proposed CCCS and VCVS method, respectively. To provide the energy storage required, a capacitor C_o is connected to the dc-link of the full-bridge converter. Like any typical power electronic converter designs, the cost, the size, and the efficiency of the system must be optimized. In the case of designing an EPI, there are two additional considerations:

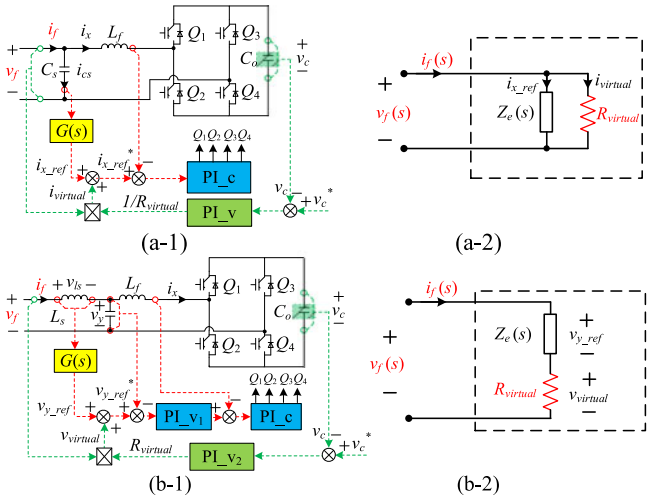

Fig. 9. Practical hardware and control implementation of an emulated power reactance based on (a-1) CCCS and (b-1) VCVS method. Their electrical equivalents are shown in (a-2) and (b-2).

1) The energy storage capability of C_o should match the actual application requirement instead of the energy storage capability of the EPI which the system is emulating.

In most ac applications, the energy storage capability of C_o should be the same as that of the power reactance which the system is emulating. For instance, if an ac capacitor with a capacitance of $C_{\rm AC}$ is emulated, which is applied in shunt with an ac grid, then C_o should be designed such that

$$C_{\rm AC}V_{f\_\rm peak}^2 = C_oV_c^2 \tag{13}$$

where $V_{f\_\rm peak}$ is the peak terminal voltage of $C_{\rm AC}$ which is equal to the ac-voltage amplitude, and V_c is the dc-link voltage of the full-bridge converter.

In dc applications, however, the required energy storage in C_o can be much smaller. This is because a dc power reactance typically stores a large portion of the redundant energy. One example is the dc-link capacitor $C_{\text{dc-link}}$ widely employed in single-phase PFC applications for reducing the double-line frequency voltage ripples [15]. It can be calculated that, with a 1% voltage ripple on the dc-link of the PFC, only 1.99% of the total energy stored in the $C_{\text{dc-link}}$ is useful for compensating the double-line frequency voltage variations, while the rest of stored energy is redundant [16]. In such applications, if an EPI is used to emulate and replace the dc-link capacitor $C_{\text{dc-link}}$, the minimum C_o should satisfy

$$\eta_E C_{\text{dc - link}}V_{f\_\rm peak}^2 = C_oV_c^2, \quad (0 < \eta_E < 1) \tag{14}$$

where η_E is energy utilization rate (which is the ratio of the useful energy to the total energy stored in $C_{\text{dc-link}}$), $V_{f\_\rm peak}$ is the peak dc-link voltage applied to $C_{\text{dc-link}}$. Some design examples for selecting C_o in PFC applications can be found in [15], [16].

2) The sensing impedance should have a negligible effect on the proper operation of the system. The incorporation of a sensing impedance, such as C_s or L_s, increases the order of the full-bridge converter. For applications in the low-frequency range (e.g., from dc up to several hundred Hertz), if C_s or L_s are sufficiently small, its effect on the overall system will be negligible. As a result, the system can still be controlled as a conventional *L* type full-bridge converter in the case of Fig. 9(a) and a *LC*-type full-bridge converter in the case of Fig. 9(b).

B. Control Strategies

The detailed control block diagrams are shown in Fig. 9(a-1) and (b-1) for the proposed CCCS- and VCVS-control methods, respectively. Compared with Fig. 4, an additional voltage-control loop for regulating v_c is included to compensate the power losses of the system.

For the CCCS [see Fig. 9(a-1)], the regulation of v_c is realized by modifying the ideal EPI (i.e., see $Z_e(s)$ in Fig. 1) into an $R_{\rm virtual} - Z_e$ parallel impedance network shown in Fig. 9(a-2). Here, $R_{\rm virtual}$ is a virtual resistor representing the overall system losses. To achieve this, the terminal voltage v_f is firstly sensed and divided by $R_{\rm virtual}$ to generate the current $i_{\rm virtual}$ through it. This current is then added to $i_{x\_\rm ref}$ to form the new reference $i_{x\_\rm ref}^*$ for the converter to track. To properly compensate the power losses, the value of $R_{\rm virtual}$ is dynamically predicted through a *PI* controller which regulates the average v_c at the target value v_c^*. This is possible because the absorbed energy, and hence, the voltage v_c varies according to the change of $R_{\rm virtual}$. Similarly, for the VSVC method given in Fig. 9(b-2), the regulation of v_c is achieved by mimicking an $R_{\rm virtual} - Z_e$ series impedance network that is achieved by sensing the terminal current i_f to derive $v_{\rm virtual}$, which is added to $v_{y\_\rm ref}$ to obtain the new reference $v_{y\_\rm ref}^*$.

The inner-loop current controller for CCCS and the voltage controller for VCVS are conventional controllers used for an *L*-type and an *LC*-type full-bridge converters. In this paper, a simple *PI* controller is used as the current controller for CCCS, and a dual-loop controller is used as the voltage controller for VCVS.

C. Bandwidth of EPI

The frequency response of an EPI can be derived by performing a closed-loop small-signal analysis over the entire system. For instance, a CCCS system can be generally modeled as shown in Fig. 10(a), where the bus voltage v_c is assumed constant (i.e., $v_c = V_c$). It can be seen that the dominating factor that limits the bandwidth of the EPI is the inner current loop's bandwidth: The higher the bandwidth of the inner current loop, the higher the EPI's bandwidth. Therefore, an optimal design of the inner current loop is necessary if high bandwidth is needed. Similarly, the limiting factor of the EPI bandwidth for a VCVS system is the inner voltage loop's bandwidth. An emulated linear capacitor based on Fig. 9(a-1) (where $G(s)$ is set to k_p) is examined here for the purpose of discussing the factors that affect the operating bandwidth of the EPI. The simplified model is shown in Fig. 10(b). Solution of the model in Fig. 10 gives the closed-loop

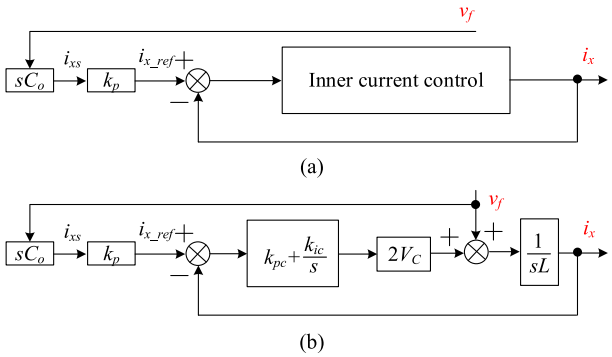

Fig. 10. (a) General and (b) simplified closed-loop small-signal system model of Fig. 9(a-1) for emulating a linear capacitor of $C_e = (k_p + 1)C_o$.

emulated impedance $Z_e(s)$ as

$$Z_e(s) = \frac{v_f(s)}{i_f(s)} = \frac{v_f(s)}{i_x(s) + i_{xs}(s)} = \frac{s^2 L_f + s(2k_{pc}V_c) + 2k_{ic}V_c}{s^3 C_o L_f + s^2(2C_o V_c k_{pc})(1+k_p) + s[1 + 2C_o(1+k_p)k_{ic}V_c]} \quad (15)$$

where k_{pc} and k_{ic} are the proportional and integral gain of the *PI* current controller, respectively.

At low frequencies, when $s \ll 1$,

$$Z_e(s)|_{s\ll 1} \approx \frac{1}{s\left[C_o(k_p+1) + \frac{1}{2k_{ic}V_c}\right]} \approx \frac{1}{sC_o(k_p+1)}, \quad (k_{ic}V_c \ll 1) \quad (16)$$

and at high frequencies,

$$Z_e(s)|_{s\to\infty} = \frac{1}{sC_o} \quad (17)$$

equations (16) and (17) indicate that the EPI is an amplified version of C_o at low frequencies and reverts to C_o at high frequencies. Fig. 11 shows the frequency response plots (in the form of admittance) of the EPI calculated based on (15). It can be observed that the EPI under test behaves like a linear capacitor of $C_e = (k_p + 1)C_o = 1010\,\mu$F only at low frequencies (up to around 2000 rad/sec). Clearly from Fig. 10(b), one can see that the bandwidth of the inner current loop is determined by (i) the PI compensator, (ii) the DC-link voltage V_c, and (iii) the output filter inductor L_f. A larger L_f tends to decrease the loop gain of the current loop. However, a larger V_c and/or an optimized compensator (including advanced nonlinear controller) design can make up for the decrease of the loop gain, resulting in a similar or even extended EPI bandwidth (assuming that the system is still stable). If the power rating of the system is very large such that a huge L_f is unavoidable, then one can either increase the switching frequency or adopt a different circuit topology, for instance, from two-level to multilevel, to reduce the filtering inductance. The output capacitor C_o, on the other hand, has nothing to do with the bandwidth of the EPI because it is not involved in the inner current loop. Instead, C_o will only offset the frequency response curve of the EPI vertically, which can be concluded from (15).

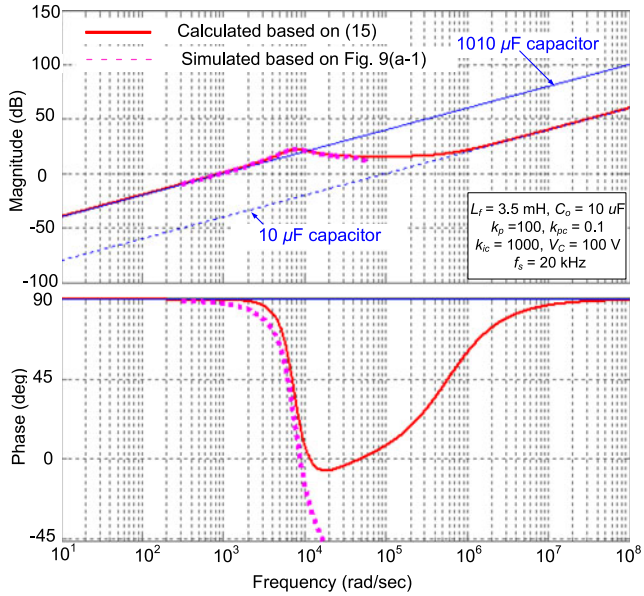

Fig. 11. Frequency response plots (in the form of admittance) of an EPI of 1010-μF capacitance value with a PI current controller [calculated based on (15)] and a PI current controller [through simulation based on the setup of Fig. 9(a-1)].

In practice, the delays due to the sampling of the analogue-to-digital converter and the computational process of the digital controller can further reduce the bandwidth of the EPI. Their effect to the bandwidth of the EPI is generally insignificant at low-frequency ranges. The simulated frequency response of the EPI that incorporates the effect of the computational and the sampling delay is shown in Fig. 11. It can be observed that the simulation model has been predicted accurately by the simplified model of (15) up to around 9000 rad/sec, beyond which the delays gradually takes over the frequency response. The sampling theorem predicts that the bandwidth an EPI cannot exceed the Nyquist frequency. Therefore, an EPI may not be suitable for applications that involve very-high-bandwidth operation.

V. Experimental Verification

A. Steady-State Performance of a Programmable Power Impedance Based on Direct Reference Generation

To evaluate the performance of an EPI based on the proposed direct reference generation method, four different experiments have been conducted. The experiments include the emulation of a linear capacitor, a linear inductor, a frequency-dependent capacitor, and a frequency-dependent inductor. The purpose of the first two experiments is to check the steady-state performance of the CCCS and VCVS method, respectively. The last two experiments are to verify the feasibility of achieving a fully programmable power impedance profile through the reconfiguration of the impedance control function $G(s)$. The hardware configuration of the EPI is the same as that shown in Fig. 9. The control of the converter is implemented using a DSP (Model:

TABLE II
DESIGN SPECIFICATIONS FOR TESTING VARIOUS EMULATED POWER REACTANCE

Design Parameter	Value	Design Parameter	Value
Average voltage for R_o	48 V	Sensing capacitor C_s	10 μF
Switching frequency f_s	25 kHz	Sensing inductor L_s	1 mH
Load R_o	100 Ω	DC-link capacitor C_o	470 μF/350 V
Filter inductor L_f	3.5 mH	Switches $Q_1 - Q_4$	IRG4PC30FDPbF

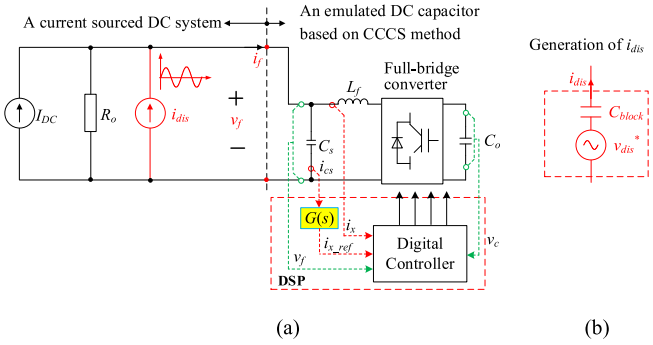

Fig. 12. (a) Experiment setup for testing the *V–I* responses of an emulated linear capacitor and a physical capacitor, and (b) a schematic diagram of $i_{\rm dis}$ generation.

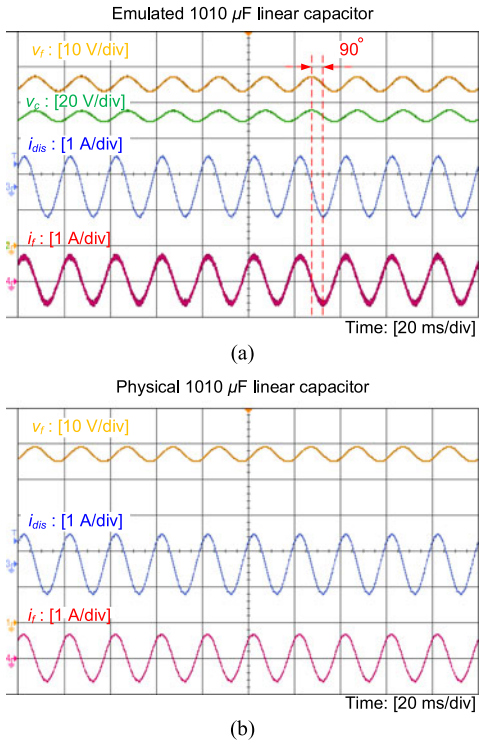

Fig. 13. Measured terminal waveforms of an emulated and a real linear capacitor of 1010-μF under 50-Hz current disturbances.

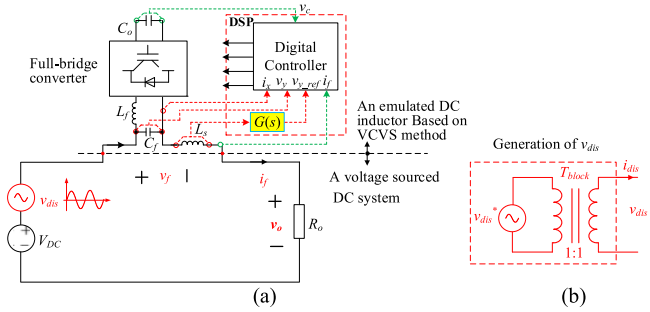

Fig. 14. Experiment setup for testing the *V–I* responses of an emulated linear inductor and a physical inductor, and (b) a schematic diagram of $v_{\rm dis}$ generation.

TMS320F28069). The detailed circuit parameters and component specifications are listed in Table II. It should be noticed that the passive components such as the dc-link capacitor, the sensing capacitor, and the filter inductor are off-the-shelf components and are selected just for the proof-of-concept of the proposed EPI. A thorough hardware optimization aiming for a higher power density and higher efficiency is intended for a future work.

1) Emulation of a DC Linear Capacitor: Fig. 12(a) shows the setup for the first experiment. A dc system comprising a dc current source $I_{\rm DC}$, a disturbing current source $i_{\rm dis}$, and a resistive load R_o are used to test the performance of an emulated dc linear capacitor. Here, $I_{\rm DC}$ is manually tuned such that the average voltage of the load R_o is 48 V. $i_{\rm dis}$ is generated by a variable-frequency dc voltage source $v_{\rm dis}^*$ (Model: GW Instek APS-9501, output frequency range 45 –500 Hz) via a 100-μF dc-voltage-blocking capacitor $C_{\rm block}$ [see Fig. 12(b)]. The frequency and amplitude of $i_{\rm dis}$ is set at 50 Hz and 0.7 A (or 0.5 Arms), respectively. The sensing capacitor C_o is chosen as 10 μF and G(s) is set as 100. According to (8), the EPI system should be emulating a linear 1010 μF capacitor.

The measured steady-state waveforms of v_f, i_f, and v_c are shown in Fig. 13(a). It can be observed that the waveforms of both i_f and v_f are purely sinusoidal. In addition, i_f is leading the ac portion of v_f by 90°. This indicates that the EPI is operating as a capacitor. For comparison, a real capacitor of 1010 μF is applied in the place of the emulated capacitor. The measured waveforms of i_f and v_f are shown in Fig. 13(b). Both v_f and i_f are almost identical for the emulated and the real capacitor. This confirms the accuracy of the emulated 1010-μF capacitor with the CCCS method at 50 Hz. Note, however, that the average voltage of v_f of the emulated capacitor is slightly lower (around 1 V) than that of the real capacitor. This is because a small portion of i_f, i.e., the dc offset current of $v_f/R_{\rm virtual}$ is used for compensating the converter power loss, and the average current through the load R_o is reduced.

2) Emulation of a DC Linear Inductor: Fig. 14(a) shows the setup for testing an emulated dc linear inductor based on the VCVS method. The dc system consists of a constant dc voltage source $V_{\rm DC}$, a disturbing voltage source $v_{\rm dis}$ (20 Vrms/50 Hz) and a resistive load R_o. Here, $V_{\rm DC}$ is manually set at 48 V, and $v_{\rm dis}$ is generated by $v_{\rm dis}^*$ through a 1:1 turns ratio isolation transformer for dc current bypassing [see Fig. 14(b)]. Since $L_o = 1$ mH and G(s) = 100, the EPI is equivalent to a linear inductor of 0.101 H.

Fig. 15(a) illustrates the measured waveforms of v_f, i_f and v_c of the emulated 0.101-H inductor. Again, pure sinusoidal waveforms are obtained and inductive operation is

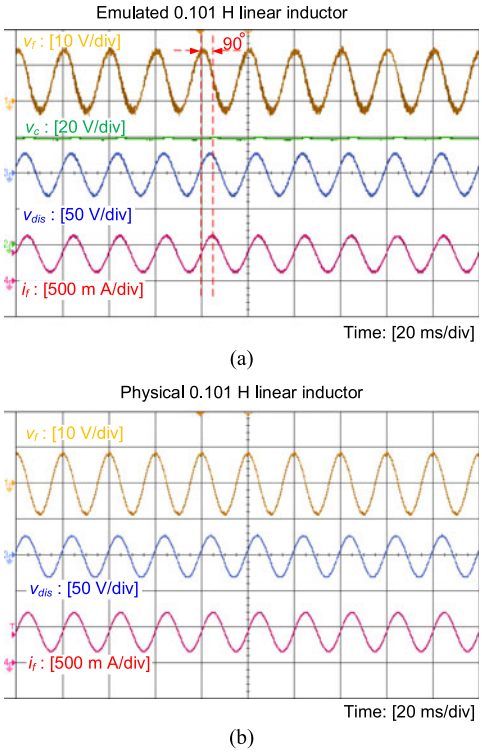

Fig. 15. Measured terminal waveforms of an emulated and a real linear inductor of 0.101 H under 50-Hz voltage disturbances.

confirmed. A second experiment is conducted by connecting a real 0.101-H inductor in the place of the emulated inductor, of which the waveforms of v_f and i_f are shown in Fig. 15(b). It is clear that the *V-I* characteristics of a physical 0.101-H inductor have been successfully emulated by the EPI based on the VCVS method.

3) Emulation of a Frequency-Dependent DC Capacitor and a Frequency-Dependent DC Inductor: The hardware setup for the third and fourth experiments are identical to those illustrated in Figs. 12 and 14. The difference is that $G(s)$ is programmed as a $P + R$ function, where $G(s) = 20 + \frac{80\times(2\times\pi\times10)s}{s^2+(2\times\pi\times10)s+(2\times\pi\times100)^2}$. Thus, the EPI should be emulating a 1010-μF capacitor and a 0.101-H inductor (101 times amplification of the sensing impedance) at 100 Hz, respectively, for the setup of Figs. 12 and 14. At other frequencies, the system should emulate a 210-μF capacitor and a 0.021-H inductor (21 times of amplification of the sensing impedance), respectively.

The measured frequency response of a linear/frequency-dependent capacitor (in the form of admittance) and a linear/frequency-dependent inductor (in the form of impedance) are shown in Fig. 16(a) and (b), respectively. Fig. 16(a) and (b) clearly confirm the feasibility of the function of $G(s)$ for controlling and manipulating the EPI.

B. Dynamic Performance of a Programmable Power Impedance as a Multifunctional Equipment

1) EPI as a Dynamic DC Linear Capacitor (Changing G(s) From a P Function to Another P Function): A dynamic linear capacitor is a linear capacitor with a variable capacitance value

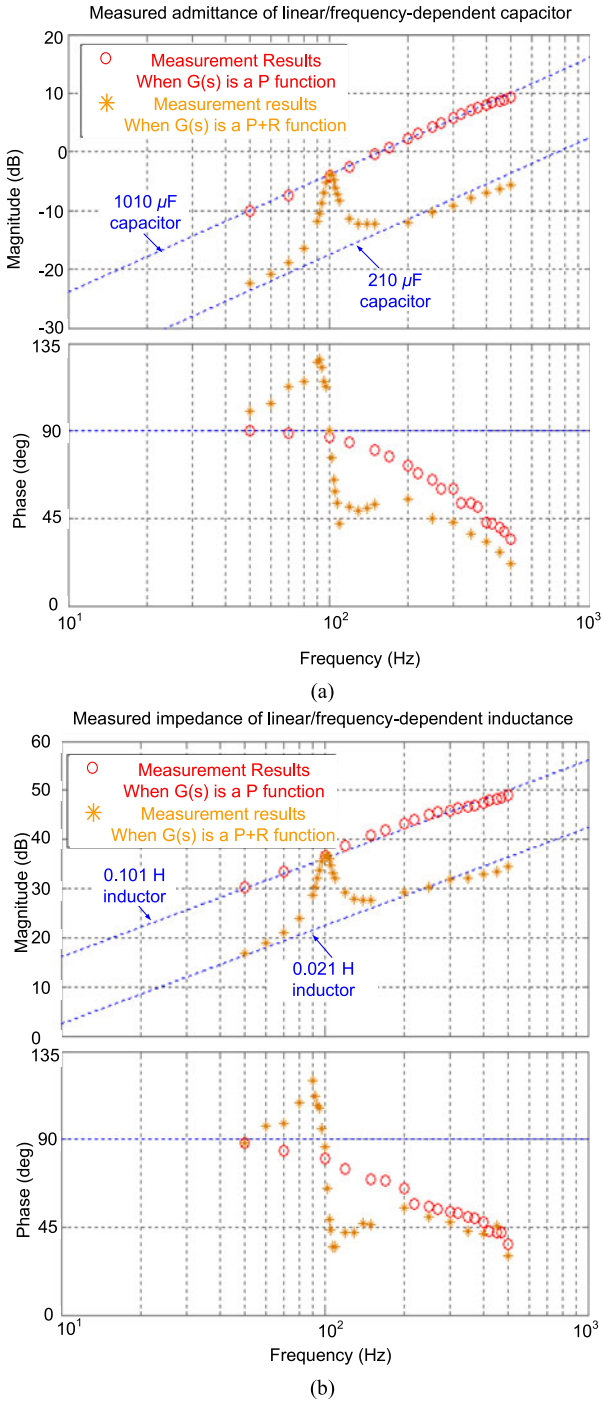

Fig. 16. Measured frequency responses of (a) a linear capacitor and a frequency-dependent capacitor, and (b) a linear inductor and a frequency-dependent inductor.

[8]. In this experiment, a dynamic dc linear capacitor is achieved by changing $G(s)$ between 0 and 20, based on the system setup shown in Fig. 12. The result will be a dynamically changing of the emulated capacitance value between 10 and 210 μF. Both ramp-change and step-change of $G(s)$ are performed and the dynamic waveforms of v_f, i_f and v_c are shown in Fig. 17(a) and (b), respectively.

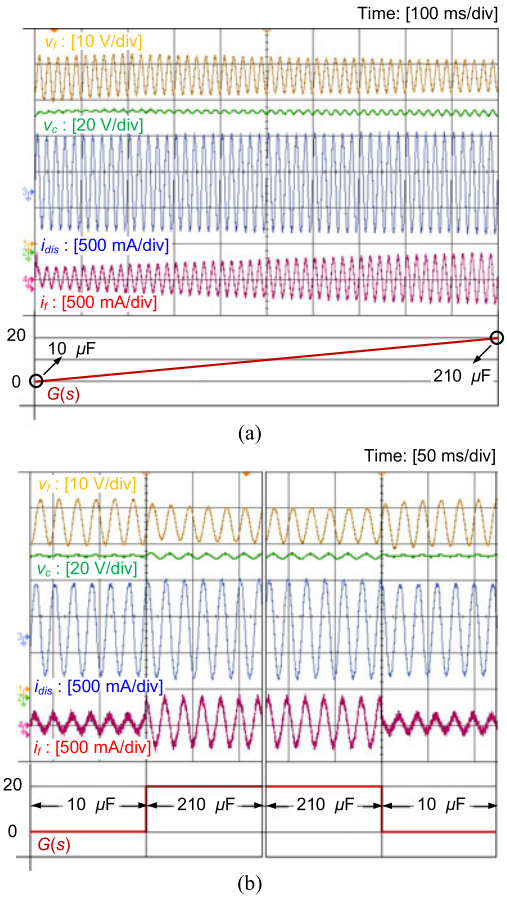

Fig. 17. Performance of the EPI as a dynamic dc linear capacitor, whose capacitance value is (a) smoothly changed and (b) stepped changed between 10 and 210 μF.

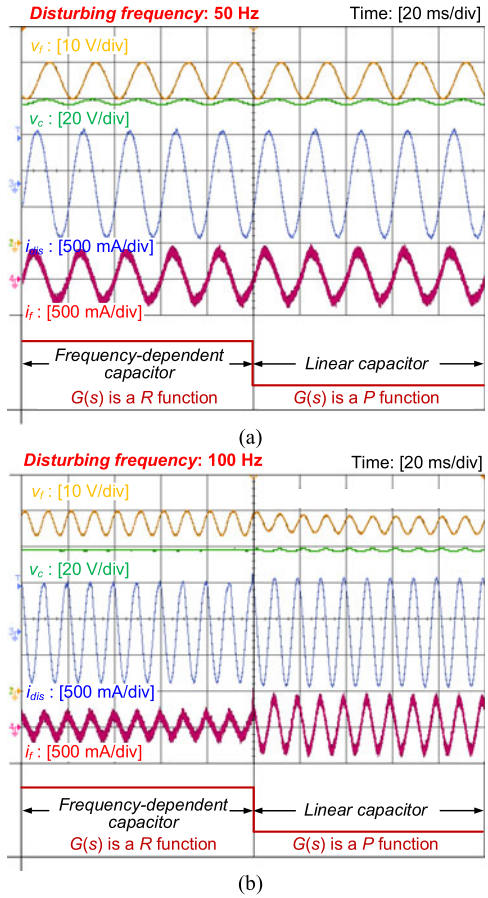

Fig. 18. Dynamic performance of the EPI, when programmed from a linear capacitor to a frequency-dependent capacitor under the condition of (a) $i_{\rm dis}$ having a frequency of 50 Hz, and (b) $i_{\rm dis}$ having a frequency of 100 Hz.

From Fig. 17(a), it can be observed that the amplitude of v_f reduces and that of i_f increases with the increase of $G(s)$. This is because the emulated capacitance increase with $G(s)$, and a larger capacitance naturally provides a better filtering function for the disturbing current $i_{\rm dis}$. For the same reason, the reactive power absorbed by the emulated linear capacitor also increases with G(s), leading to an increasing amplitude of v_c. In Fig. 17(b), $G(s)$ is step changed from 20 to 0 and then back to 20. The emulated capacitance is changed almost instantly with the change of $G(s)$. This can be observed by inspecting the waveforms of v_f, i_f, or v_c. The amplitudes of these waveforms are instantly changed with the change of $G(s)$.

2) EPI as a Plug-and-Play Ripple Mitigator (Changing G(s) From R Function to P Function): A plug-and-play ripple mitigator is a device which has a low impedance only at selective frequencies, while it has an infinitely large impedance at dc [17]. This can be achieved by programming the EPI as a frequency-dependent capacitor, i.e., configuring $G(s)$ in Fig. 12 into an *R* function. To demonstrate the frequency-dependent *V–I* characteristics of the EPI, two similar experiments are conducted and the results are shown in Fig. 18. In both experiments, $G(s)$ is changed from an *R* function $\left(G(s)\frac{20\times(2\times\pi\times10)s}{s^2+(2\times\pi\times10)s+(2\times\pi\times50)^2}\right)$ to a *P* function $(G(s) = 20)$. The frequency of the disturbing current $i_{\rm dis}$ is set at 50 and 100 Hz in Fig. 18(a) and (b), respectively. Based on the *R* and the *P* function configured, the EPI is always emulating a 210-μF capacitor at 50 Hz (11 times of the amplification of C_o) before and after the step change. Therefore, the waveforms of v_f, i_f, and v_c remain in Fig. 18(a), when the type of the impedance is changed. At 100 Hz, however, the filtering effect of the EPI based on the *R* and the *P* function becomes different, as clearly indicated Fig. 18(b). These results confirm that an EPI based on an *R* function has a frequency-dependent capacitance value. The results also demonstrate that a fast changing between an emulated linear capacitor and a frequency-dependent capacitor is viable.

3) EPI as a Negative Capacitor (Changing G(s) From P Function to −P Function): A negative capacitor can be achieved by configuring $G(s)$ as a –*P* function. In this experiment, an extra dc capacitor of 200 μF is connected in a shunt with the load R_o (not shown in Fig. 12) to test the performance of a negative capacitor. The use of the extra capacitor in the system is to ensure a positive overall capacitance in the system, in order to guarantee a stable system operation. The reason is analogue to that explained in [14] for a negative inductor.

When $G(s)$ is smoothly changing from 20 to -20 as shown in Fig. 19, the EPI is emulating a capacitor with a capacitance value between 210 to -190 μF. Considering the extra added 200-μF capacitor, the total capacitance value of the dc system

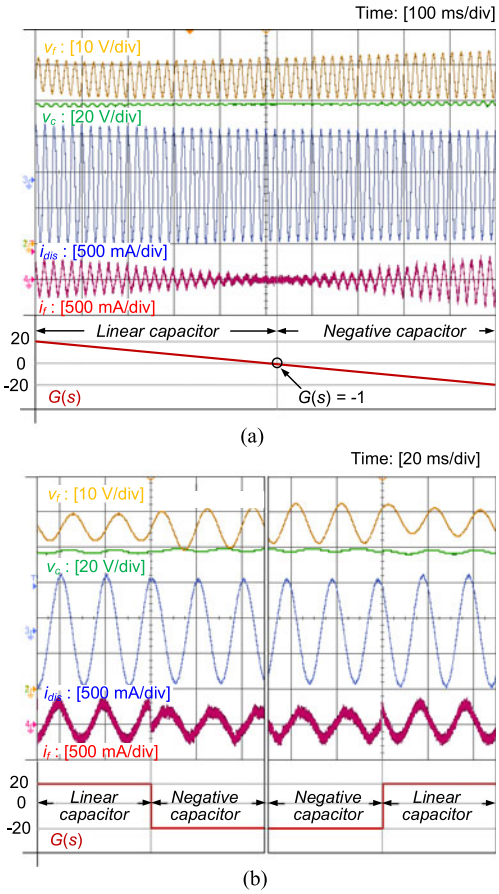

Fig. 19. Dynamic performance of the EPI when programmed from a linear capacitor to a negative capacitor. The capacitance value is changed smoothly in (a) and is step changed in (b) from 210 to -190 μF.

varies between 410 to 10 μF. As the total capacitance of the dc system decreases, the amplitude of v_f increases. An interesting phenomenon can be observed before and after $G(s)$ passes the negative unity gain point (i.e., $G(s) = -1$): $i_{\rm f}$ is leading the ac portion of v_f by 90° when $G(s) > -1$, and i_f is lagging the ac portion of v_f by 90° when $G(s) < -1$. These results show that a negative capacitor has the same steady-state *V–I* characteristics as an inductor. In Fig. 19(b), a test of step change of G(s) between 20 to -20 is conducted. It can be seen that a fast transition between a linear capacitor and a negative capacitor has been achieved.

4) EPI as a SVC (Changing G(s) From R Function to $-R$ Function): An SVC can be regarded as a type of dynamic frequency-dependent reactance, of which both inductive and capacitive reactive power generation needs to be generated. To achieve reactive power generation for a 50-Hz system, $G(s)$ is set as an R function $(\frac{(2\times\pi\times10)s}{s^2+(2\times\pi\times10)s+(2\times\pi\times50)^2})$, which has a unity gain at 50 Hz. Variable capacitive power generation can be achieved by configuring the gain of the R function to be larger than -1, whereas inductive power generation can be achieved when the gain of the R function is less than -1. A miniature 20-Vrms/ 50-Hz ac system powered by an ac voltage source $V_{\rm AC}$ is used to test the performance of the EPI (see Fig. 20). Note that the hardware of the EPI is identical to that used in Fig. 12.

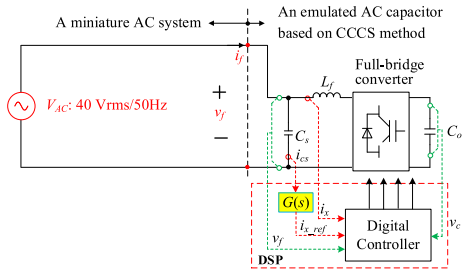

Fig. 20. Experiment setup for testing the dynamic performance of an EPI as an SPC.

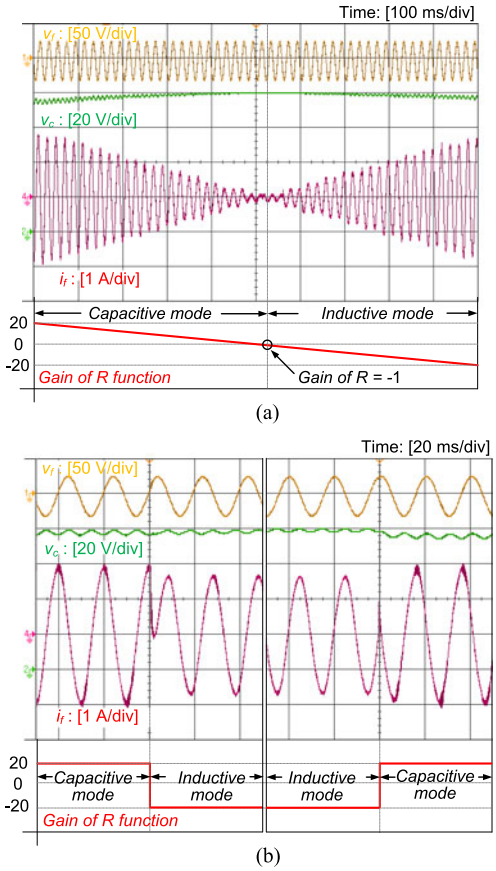

Fig. 21. Dynamic performance of the EPI when changed from a frequency-dependent capacitor to a frequency-dependent inductor. The gain of the R function is changed smoothly in (a) and is step changed in (b) between 10 to -10.

Fig. 21 shows the measured v_f and i_f, when the gain of the R function changes between 20 and -20. As the gain of the R function passes the -1 point in Fig. 21(a), the phase relationship between i_f and v_f also changes from leading 90° to lagging 90°. In addition, as the gain of R gradually reduces, the reactive current i_f, and hence, the produced reactive power changes linearly and seamlessly. In Fig. 21(b), when the gain of the R function is step changed from 20 to -20 or inversely, the phase of i_f with respect to v_f is changed instantly. Therefore, fast switching between a frequency-dependent capacitor/inductor has been demonstrated. The results indicate that a fast dynamic SVC based on direct impedance control is feasible.

VI. Conclusion

In this paper, a general control strategy for actuating a programmable and reconfigurable power impedance is presented. The challenges, control method, and practical considerations are explained. A programmable power reactance which can be configured as a linear capacitor, a negative capacitor, a frequency-dependent capacitor, or a frequency-dependent inductor, has been successfully demonstrated and tested in hardware using a full-bridge inverter with small passive reactive components. With the proposed control method, fast changing between different reactance values and types is feasible. The control method can be further extended to emulate a general form of the power impedance, provided that the power converter is capable of both real and reactive power generation. Unlike the existing EPIs which are designed specifically for a single task, the programmable EPI here can achieve multiple functions according to the user input. The concept of programmable EPI may offer a new and flexible way to perform power filtering, energy storage, and even power conversion from an impedance perspective. It is believed by the authors that the concept of EPI should be further explored in applications such as active filtering, SVC, power flow control [18], ancillary serves [19], hardware-in-the-loop, power system stability [20], single-phase AC/DC converters without electrolytic capacitors [21]–[25], and lighting [26].

References

[1] Power Electronics Group California Institute of Technology, "Input-current shaped AC-to-DC converters," NASA Lewis Res. Center, Cleveland, OH, USA, Rep. NASA-CE- 176767, 1986.

[2] H. Funato and A. Kawamura, "Proposal of variable active-passive reactance," in *Proc. Int. Conf. Ind. Electron., Control, Instrum. Autom.*, 1992, pp. 381–388.

[3] O. Kirshenboim, A. Cervera, B. Halivni, E. Abramov, and M. M. Peretz, "Plug-and-play electronic capacitor for VRM applications," in *Proc. IEEE Appl. Power Electron. Conf. Expo.*, 2016, pp. 111–117.

[4] D. Rana, B. Hafez, P. Garg, S. Essakiappan, and P. Enjeti, "Analysis and design of active inductor as DC-link reactor for lightweight adjustable speed drive systems," in *Proc. IEEE Energy Convers. Congr. Expo.*, 2014, pp. 3243–3250.

[5] C. C. Yang, Y. L. Chen, and Y. M. Chen, "Active capacitor with ripple-based duty cycle modulation for AC-DC applications," in *Proc. IEEE Appl. Power Electron. Conf. Expo.*, 2016, pp. 558–563.

[6] S.-Y. Lee, Y.-L. Chen, Y.-M. Chen, and K. H. Liu, "Development of the active capacitor for PFC converters," in *Proc. IEEE Energy Convers. Congr. Expo.*, 2014, pp. 1522–1527.

[7] B. Liu, S. Zhang, S. Zheng, Y. Ma, F. Wang, and L. M. Tolbert, "Design consideration of converter based transmission line emulation," in *Proc. IEEE Appl. Power Electron. Conf. Expo.*, 2016, pp. 966–973.

[8] X. Zhang, X. Ruan, H. Kim, and C. K. Tse, "Adaptive active capacitor converter for improving stability of cascaded DC power supply system," *IEEE Trans. Power Electron.*, vol. 28, no. 4, pp. 1807–1816, Apr. 2013.

[9] X. Chen, K. Dai, C. Xu, Z. Dai, and L. Peng, "Reactive power compensation with improvement of current waveform quality for single-phase buck-type dynamic capacitor," in *Proc. IEEE Appl. Power Electron. Conf. Expo.*, 2016, pp. 1358–1363.

[10] S. Inoue, T. Shimizu, and K. Wada, "Control methods and compensation characteristics of a series active filter for a neutral conductor," *IEEE Trans. Ind. Electron.*, vol. 54, no. 1, pp. 433–440, Feb. 2007.

[11] A. Nabae, Y. Nakajima, L. Cao, T. Tanaka, and S. Ariga, "A series active capacitance for compensating voltage drops caused by source impedances in power systems," in *Proc. IEEE Power Electron. Specialists Conf.*, 1997, vol. 1, pp. 351–355.

[12] J. C. P. Liu, C. K. Tse, F. N. K. Poon, M. H. Pong, and Y. M. Lai, *Int. J. Circuit Theory Appl.*, vol. 36, no. 3, pp. 275–287, 2008.

[13] B. Liu, S. Zheng, Y. Ma, F. Wang, and L. M. Tolbert, "Control and implementation of converter based ac transmission line emulation," in *Proc. IEEE Appl. Power Electron. Conf. Expo.*, 2015, pp. 1807–1814.

[14] H. Funato, A. Kawamura, and K. Kamiyama, "Realization of negative inductance using variable active-passive reactance (VAPAR)," *IEEE Trans. Power Electron.*, vol. 12, no. 4, pp. 589–596, Jul. 1997.

[15] S. Wang, X. Ruan, K. Yao, S.-C. Tan, Y. Yang, and Z. Ye, "A flicker-free electrolytic capacitor-less AC–DC LED driver," *IEEE Trans. Power Electron.*, vol. 27, no. 11, pp. 4540–4548, Nov. 2012.

[16] W. Qi, H. Wang, X. Tan, G. Wang, and K. D. T. Ngo, "A novel active power decoupling single-phase PWM rectifier topology," in *Proc. IEEE Appl. Power Electron. Conf. Expo.*, 2014, pp. 89–95.

[17] S. Li, A. T. L. Lee, S. C. Tan, and S. Y. R. Hui, "A plug-and-play ripple mitigation approach for DC-links in hybrid systems," in *Proc. Appl. Power Electron. Conf. Expo.*, 2016, pp. 169–176.

[18] X. Wang, Y. W. Li, F. Blaabjerg, and P. C. Loh, "Virtual-impedance-based control for voltage-source and current-source converters," *IEEE Trans. Power Electron.*, vol. 30, no. 12, pp. 7019–7037, Dec. 2015.

[19] J. He and Y. W. Li, "Analysis, Design, and Implementation of Virtual Impedance for Power Electronics Interfaced Distributed Generation," *IEEE Trans. Ind. Appl.*, vol. 47, no. 6, pp. 2525–2538, Nov. 2011.

[20] L. Harnefors, X. Wang, A. G. Yepes, and F. Blaabjerg, "Passivity-Based Stability Assessment of Grid-Connected VSCs-An Overview," *IEEE J. Emerg. Sel. Top. Power Electron.*, vol. 4, no. 1, pp. 116–125, Mar. 2016.

[21] A. S. Morsy and P. N. Enjeti, "Comparison of active power decoupling methods for high-power-density single-phase inverters using wide-bandgap FETs for Google Little Box challenge," *IEEE J. Emerg. Sel. Top. Power Electron.*, vol. 4, no. 3, pp. 790–798, Sep. 2016.

[22] M. A. Vitorino, L. F. S. Alves, R. Wang, and M. B. de Rossiter Correa, "Low-Frequency Power Decoupling in Single-Phase Applications: A Comprehensive Overview," *IEEE Trans. Power Electron.*, vol. 32, no. 4, pp. 2892–2912, Apr. 2017.

[23] S. Li, G.-R. Zhu, S.-C. Tan, and S. Y. R. Hui, "Direct ac/dc rectifier with mitigated low-frequency ripple through inductor-current waveform control," *IEEE Trans. Power Electron.*, vol. 30, no. 8, pp. 4336–4348, Aug. 2015.

[24] S. Li, W. Qi, S.-C. Tan, and S. Y. R. Hui, "Integration of an Active Filter and a Single-Phase AC/DC Converter With Reduced Capacitance Requirement and Component Count," *IEEE Trans. Power Electron.*, vol. 31, no. 6, pp. 4121–4137, Jun. 2016.

[25] S. Li, W. Qi, S.-C. Tan, and S. Y. Hui, "A Single-Stage Two-Switch PFC Rectifier with Wide Output Voltage Range and Automatic AC Ripple Power Decoupling," *IEEE Trans. Power Electron.*, pp. 1–1, 2016.

[26] S. Li, S.-C. Tan, C. K. Lee, E. Waffenschmidt, S. Y. Hui, and C. Tse, "A survey, classification and critical review of light-emitting diode drivers," *IEEE Trans. Power Electron.*, vol. 31, no. 2, pp. 1503–1516, 2015.

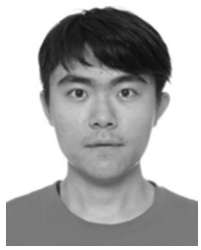

Sinan Li (M'14) received the B.S. degree in electrical engineering from the Harbin Institute of Technology, Sheng, China, in 2009, and the Ph.D. degree in electrical and electronic engineering from The University of Hong Kong, Hong Kong, in 2014.

He is currently a Postdoctoral Fellow at the Department of Electrical and Electronic Engineering, The University of Hong Kong. He has authored more than 30 transaction papers and conference papers. He also holds three U.S. patents. His current research areas include the power electronics, LED lighting, control, renewable energy and smart grids.

Dr. Li is one of the Founding Members of IEEE-Eta Kappa Nu (HKN) at The University of Hong Kong.

Wenlong Qi (S'14) received the B.E. and M.E. degrees in electrical and electronic engineering from the Shandong University, Jinan, China, in 2011 and 2014, respectively. He is currently working toward the Ph.D. degree in the Department of Electrical and Electronic Engineering, The University of Hong Kong, Hong Kong.

His research interests include single-phase ac/dc, dc/ac converter, and nonlinear control technique.

Siew-Chong Tan (S'00–M'06–SM'11) received the B.Eng. (Hons.) and M.Eng. degrees in electrical and computer engineering from the National University of Singapore, Singapore, in 2000 and 2002, respectively, and the Ph.D. degree in electronic and information engineering from Hong Kong Polytechnic University, Hung Hom, Hong Kong, in 2005.

From October 2005 to May 2012, he was a Research Associate, a Postdoctoral Fellow, a Lecturer, and an Assistant Professor in the Department of Electronic and Information Engineering, Hong Kong Polytechnic University. From January to October 2011, he was Senior Scientist with the Agency for Science, Technology and Research (A∗Star), Singapore. He was a Visiting Scholar with Grainger Center for Electric Machinery and Electromechanics, University of Illinois at Urbana-Champaign, Champaign, USA, from September to October 2009, and an Invited Academic Visitor with the Huazhong University of Science and Technology, Wuhan, China, in December 2011. He is a coauthor of the book Sliding Mode Control of Switching Power Converters: Techniques and Implementation (CRC, 2011). His research interests include the areas of power electronics and control, LED lightings, smart grids, and clean energy technologies.

Dr. Tan serves extensively as a reviewer for various IEEE/IET transactions and journals on power, electronics, circuits, and control engineering.

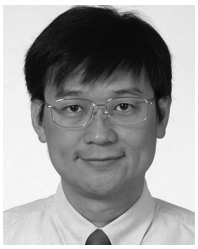

S. Y. (Ron) Hui (M'87–SM'94–F'03) received the B.Sc. (Eng. Hons.) from the University of Birmingham, Birmingham, U.K., in 1984, and the D.I.C. and Ph.D. degrees in electrical and electronic engineering from Imperial College London, London, U.K., both in 1987.

He has previously held academic positions at the University of Nottingham from 1987 to 1990, University of Technology Sydney from 1991 to 1992, University of Sydney from 1992 to 1996, and City University of Hong Kong from 1996 to 2011. Since July 2011, he has been the Chair Professor at the University of Hong Kong, Pokfulam, Hong Kong, and also at Imperial College London, since July 2010. He has published more than 200 technical papers, including more than 150 refereed journal publications and book chapters. More than 50 of his patents have been adopted by industry.

Dr. Hui is a Fellow of IET. He has been an Associate Editor of the IEEE TRANSACTIONS ON POWER ELECTRONICS, since 1997, and an Associate Editor of the IEEE TRANSACTIONS ON INDUSTRIAL ELECTRONICS, since 2007. He received twice the IEEE Distinguished Lecturer Award by the IEEE Power Electronics Society in 2004 and 2006. He was one of the 18 Administrative Committee members of the IEEE Power Electronics Society and the Chairman of its Constitution and Bylaws Committee from 2002 to 2010. He received the Excellent Teaching Award at CityU in 1998 and the Earth Champion Award in 2008. He received the IEEE Best Paper Award from the IEEE IAS Committee on Production and Applications of Light in 2002, and two IEEE Power Electronics Transactions Prize Paper Awards for his publications on Wireless Charging Platform Technology in 2009, and on LED System Theory in 2010. His inventions on wireless charging platform technology underpin key dimensions of Qi, the world's first wireless power standard, with freedom of positioning and localized charging features for wireless charging of consumer electronics. In Nov. 2010, he received the IEEE Rudolf Chope R&D Award from the IEEE Industrial Electronics Society, the IET Achievement Medal (The Crompton Medal), and was elected to the Fellowship of the Australian Academy of Technological Sciences and Engineering.

Chi K. Tse (M'90–SM'97–F'06) received the B.Eng. (Hons.) degree with first class honors in electrical engineering and the Ph.D. degree in electrical engineering from the University of Melbourne, Parkville, Australia, in 1987 and 1991, respectively.

He is currently the Chair Professor of Electronic Engineering at the Hong Kong Polytechnic University Hung Hom, Hong Kong, where he was the Head of the Department of Electronic and Information Engineering from 2005 to 2012. In 2011, he was appointed the Honorary Professor by RMIT University, Melbourne, Australia. His research interests include complex network applications, power electronics, and chaos-based communications.

Dr. Tse is the Editor-in-Chief of the IEEE CIRCUITS AND SYSTEMS MAGAZINE and the Editor-in-Chief of the IEEE CIRCUITS AND SYSTEMS SOCIETY NEWSLETTER. He was/is an Associate Editor for the IEEE TRANSACTIONS ON CIRCUITS AND SYSTEMS PART I—FUNDAMENTAL THEORY AND APPLICATIONS from 1999 to 2001 and again from 2007 to 2009. He has also been an Associate Editor for the IEEE TRANSACTIONS ON POWER ELECTRONICS since 1999. He is an Editor of the *International Journal of Circuit Theory and Applications* and is an honorary member of the Editorial Board of the *International Journal and Bifurcation and Chaos*. He received the L.R. East Prize from the Institution of Engineers, Australia, in 1987, the Best Paper Award from IEEE TRANSACTIONS ON POWER ELECTRONICS in 2001, the Best Paper Award from *International Journal of Circuit Theory and Applications* in 2003, the IEEE Distinguished Lecturer Award in 2005 and 2011, the Distinguished International Research Fellowship by the University of Calgary, Canada, in 2007. In 2009 and 2013, he and his co-inventors won the Gold Medal at the International Exhibition of Inventions of Geneva, Switzerland, on LED lighting technologies. He was awarded the Gledden Fellowship and the Distinguished International Fellowship, in 2013 and 2015, respectively, by the University of Western Australia, Perth, Australia.